ACS APPLIED MATERIALS & INTERFACES

Research Article

www.acsami.org

Low Temperature Aqueous Electrodeposited TiO_x Thin Films as Electron Extraction Layer for Efficient Inverted Organic Solar Cells

Kim Hai Wong,*[,†,‡] Chad William Mason,[†,⊥] Sappani Devaraj,[†,∥] Jianyong Ouyang,*[,§] and Palani Balaya*[,†]

[†]Department of Mechanical Engineering, National University of Singapore, 9 Engineering Drive 1, Singapore 117576, Singapore

[‡]Solar Energy Research Institute of Singapore, National University of Singapore, 7 Engineering Drive 1, Singapore 117574, Singapore

[§]Department of Material Science and Engineering, National University of Singapore, 9 Engineering Drive 1, Singapore 117576, Singapore

Supporting Information

ABSTRACT: Organic solar cells based on poly(3-hexylthiophene) and [6,6]-phenyl-C_{61}-butyric acid methyl ester were fabricated with electrodeposited TiO_x electron extraction layers 5−180 nm thick. Electrodeposition under ambient conditions is an attractive, facile and viable approach to prepare metal oxide interfacial layers. The TiO_x films obtained displayed a linear relationship between thickness and deposition time when fabricated under ambient conditions using an aqueous air stable peroxotitanium precursor. The precursor solution was prepared from titanium isopropoxide using a chelate process, which allowed water to be used as solvent due to considerably decreased sensitivity of the precursor solution towards hydrolysis. Highly conformal TiO_x films, typically observed with vacuum deposition techniques, were obtained on the indium tin oxide substrate upon electrogeneration of OH^- ions using H_2O_2 additive. Conversely, significantly rougher films with spherical growths were obtained using NO_3^- additives. Low temperature annealing at 200 °C in air was found to greatly improve purity and O stoichiometry of the TiO_x films, enabling efficient devices incorporating the electrodeposited TiO_x to be made. Using MoO_x as the hole extraction layer, the maximum power conversion efficiency obtained was 3.8% (V_{oc} = 610 mV; J_{sc} = 10.6 mA/cm^2; FF = 59%) under simulated 100 mW/cm^2 (AM1.5G) solar irradiation, whereas an efficiency of 3.4% was achieved with fully solution processed interfacial layers comprising the electrodeposited TiO_x films and a surfactant-modified PEDOT:PSS hole extraction layer.

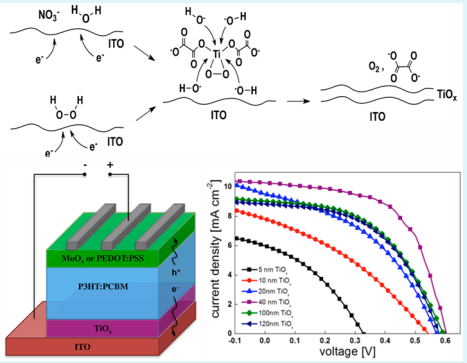

KEYWORDS: *Electrodeposition, inverted organic photovoltaic, titanium oxide, thin film, solution processed, morphology*

INTRODUCTION

Organic photovoltaics (OPVs) represent an important class of solar technology that utilizes conjugated organic molecules to capture and convert solar energy into electricity.[1] Current interest in OPV research is strong due to the commercialization potential of this technology as a low cost alternative to mainstream solar cell technologies. Portable electronics featuring lightweight and flexible OPVs have been demonstrated in recent years using scalable cost effective techniques.[2−5]

Charge selective interfacial layers are critical components in OPVs that provide an intermediary energy step between the bulk heterojunction (BHJ) and a metallic contact, so that a charge selective pathway to the external circuit for one of the two charge carriers in the photoactive layer is formed.[6−8] Typically, the transparent tin-doped indium oxide (ITO) substrate is modified with a hole extraction layer (HEL) so that ITO assumes the role of the anode where holes are extracted (Figure 1). By depositing an electron extraction layer (EEL) on ITO, however, the substrate is modified into the device cathode, resulting in a reversed current flow and a device architecture known as the inverted OPV (*i*OPV) (Figure 1). *i*OPVs exhibit distinct improvements in lifetime over conventional OPVs because (1) low work function metals that oxidize readily, such as Ca typically used in metalizing conventional OPVs, are avoided and (2) the acidic poly(3,4-ethylenedioxythiophene):poly(styrenesulfonate) (PEDOT:PSS) HEL is not in direct contact with ITO, thus preventing PEDOT:PSS-induced etching that is known to be detrimental to device lifetime.[9−13]

Metal oxide interfacial layers are robust films with the desirable optoelectronic properties and ambient stability required for fabrication of efficient and stable *i*OPVs. Although both vacuum and wet deposition processes for metal oxide EEL have been reported in literature, the latter stands out because metal oxides, such as TiO_x, are readily formed through sol−gel or nanoparticle approaches.[12−26] Electrodeposition is an attractive route for facile and potentially scalable fabrication

Received: November 18, 2013
Accepted: January 31, 2014
Published: January 31, 2014

   dx.doi.org/10.1021/am405193r | *ACS Appl. Mater. Interfaces* 2014, 6, 2679−2685

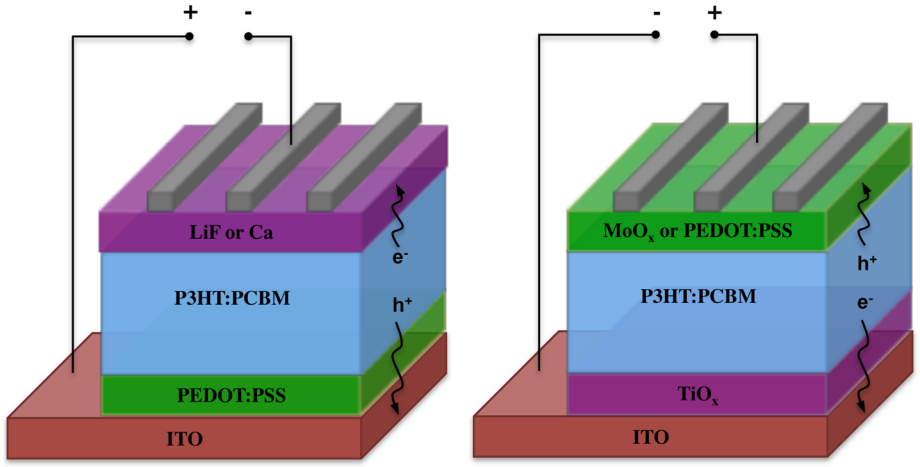

Figure 1. Schematic representations of the conventional (left) and inverted (right) OPV device structures.

of metal oxide films. It enables metal oxide films of various properties to be prepared. In this regard, three main approaches have been reported in literature:[27−31] (1) electrochemical oxidation/reduction of a precursor to yield the oxide, (2) electrophoretic deposition (colloidal oxide particles homogenously dispersed in a liquid migrate and deposit onto an electrode under the influence of an applied electric field), and (3) electroprecipitation of the oxide due to a local change in pH at the working electrode caused by electrochemically generated H^+ or OH^- ions. These approaches have been used successfully to fabricate relatively thick and porous TiO_x films for various applications.[32−36] Thin and dense TiO_x films (<200 nm) obtained by electrodeposition for OPV application, however, have not been reported. In the case of Ti(IV) compounds, electrodeposition by reduction of a precursor containing Ti in a higher oxidation state is unsuitable as such precursors are highly unstable whereas porosity of electropherotic deposited films are incompatible with the low thickness requirements of OPV interfacial layers. Therefore, electroprecipitation is preferred for TiO_x EEL fabrication in this study.

Herein, we report the cathodic electroprecipitation of TiO_x EEL at ambient conditions using an aqueous, air stable peroxotitanium oxalate precursor. The precursor solution was prepared from titanium isopropoxide using a chelate process, which in contrast to the established sol−gel approach, allowed water to be used as solvent due to considerably decreased sensitivity of the precursor solution towards hydrolysis (it should be noted that any oxygen containing ligand such as citrates, tartrates, ascorbates, nitrates, sulphates, etc. are suitable capping agents). The synthesis route involves raising pH at the ITO working electrode with electrogenerated hydroxyl ions (OH^-) that liberate the oxalate ligands and precipitate TiO_x. Unlike SO_4^{2-} ligands previously reported,[33,37] the oxalate ligands used here can be effectively removed at low temperature (200 °C) to ensure process compatibility with flexible plastic substrates such as polyethylene naphthalate (PEN) and polyethylene terephthalate (PET). It was shown that the TiO_x EEL could be made highly conformal to the substrate morphology when hydrogen peroxide (H_2O_2) was used as the additive for OH^- electrogeneration. Conversely, significantly rougher films with spherical growths were obtained using NO_3^- additives across various thicknesses, suggesting that the choice of additive has a significant impact on film morphology. Device results based on the poly(3-hexylthiophene) (P3HT) donor and [6,6]-phenyl-C_{61} butyric acid methyl ester (PCBM), MoO_x HEL as well as PEDOT:PSS HEL are discussed.

EXPERIMENTAL SECTION

Materials. All chemicals were used as purchased without further purification. Anhydrous titanium isopropoxide ($Ti(iOPr)_4$), PCBM, *ortho*-dichlorobenzene (*o*-DCB), and Al were purchased from Sigma Aldrich. Oxalic acid ($H_2C_2O_4$), H_2O_2, ammonium hydroxide (NH_4OH), and P3HT were obtained from Alfa Aesar, Merck, Fluka and Rieke Metals, respectively.

Precursor Synthesis. The 10 mM peroxotitanium oxalate precursor was prepared by dissolving an appropriate amount of $Ti(iOPr)_4$ in a strong aqueous solution of $H_2C_2O_4$ and ultrasonicated until all precipitates formed by hydrolysis of $Ti(iOPr)_4$ in water were completely dissolved. The pH of the precursor solution was adjusted by adding NH_4OH drop wise. In optimizing the pH of the precursor, little or no deposition with significantly long deposition times were observed when pH was less than 4.5 (presumably because electrogenerated OH^- ions would be rapidly neutralized) whereas spontaneous precipitation occurred when pH was greater than 4.5 (depending on the pH, this may be instantaneous or take a few days). An optimum pH of 4.5 was thus defined in this study. Equimolar H_2O_2 was subsequently added to obtain an orange-yellow peroxotitanium oxalate solution. Finally, excess H_2O_2 or $NaNO_3$ was added as additive at a mole ratio of 1:2 with respect to $Ti(iOPr)_4$ concentrations, to allow electrogeneration of OH^-. This precursor was found suitable for use up to 5 days when stored in a shaded and cool environment. It should be noted that any amorphous TiO_2 source may be used in place of $Ti(iOPr)_4$. Preparation of the precursor can be described as follows:[37,38]

$$Ti(iOPr)_4 + 4H_2O \rightarrow Ti(OH)_4 + 4PrOH(propanol)$$

$$Ti(OH)_4 + 2H_2C_2O_4 \rightarrow 2H^+ + TiO(C_2O_4)_2^{2-} + 3H_2O$$

$$TiO(C_2O_4)_2^{2-} + H_2O_2 \rightarrow Ti(O_2)(C_2O_4)_2^{2-}(orange\text{-}red) + H_2O$$

TiO_x Electrodeposition and Device Fabrication. Potentiostatic electrodeposition was performed at −1.2 V with ITO as working electrode, a saturated calomel (SCE) reference electrode (Hanna Instruments) and a Pt-foil counter electrode (MetroOhm) (Supporting Information, Figure S1). The ITO substrates (20 Ω/sq, Xinyan Technology Ltd) were cleaned by successive ultrasonication in detergent, DI water, acetone and isopropyl alcohol for 20 min each, dried with a N_2 air gun and treated with a 20 min UV−O_3 treatment before use.

By controlling the voltage pulse period, the thickness of the TiO_x film was found to vary linearly with deposition time. Films between 5

dx.doi.org/10.1021/am405193r | ACS Appl. Mater. Interfaces 2014, 6, 2679−2685

and 180 nm were prepared for this study (Figure 2). As-deposited films were subsequently annealed at 200 °C in air for 30 min before

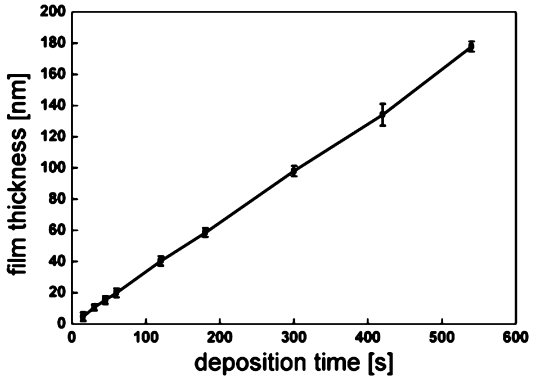

Figure 2. TiO_x films obtained showed a linear relationship with the applied potential duration used in this study.

transferring into a N_2 atmosphere glovebox (O_2 and H_2O < 1 ppm). The active layer was prepared by spin coating a filtered solution (0.45 μm Titan2 PTFE filter) consisting 1:0.8 (w/w) 22 mg mL^{-1} P3HT:PCBM blend dissolved in *o*-DCB. The P3HT:PCBM films were then dried at 140 °C for 7 min and had a thickness of 200 nm. The devices were completed by sequential thermal evaporation of MoO_3 and Al at 0.2 Å s^{-1} and 1−3 Å s^{-1}, respectively, in a chamber at 1−1.5 × 10^{-6} mbar without breaking vacuum. Alternatively, PEDOT:PSS was spin coated on the active layer in place of evaporated MoO_x. The PEDOT:PSS solution was modified with 5% (v/v) Capstone FS-31 fluorosurfactant to encourage wettability over the hydrophobic active layer.[39] A shadow mask was used to complete four devices per substrate with areas of 0.11 cm^2 each. Devices were encapsulated with UV-cured epoxy and glass in the glovebox before testing.

Characterization. Photovoltaic tests were performed in air under a calibrated solar simulator with an irradiation of 100 mW cm^{-2} at air mass 1.5 global (AM 1.5 G). Current density−voltage (J−V) characteristics were measured using a Keithley 2420 source meter. X-ray photoelectron spectroscopy (XPS) was performed using monochromatized Al Kα at 1486.71 eV on a Kratos AXIS UltraDLD system. The results were calibrated with reference to the C1s emission peak (C−C) at 284.5 eV. Curve-fitting was performed using a combination of Gaussian and Lorentzian curves (Voigt type plot). An atomic force microscope (AFM) operated in tapping mode was used to measure film roughness.

RESULTS AND DISCUSSION

Elemental Analysis. Titanium oxides have been reported to precipitate from solutions of oxo- and peroxotitanium complexes through the influence of OH^- ions.[40] The necessity of OH^- ions for successful oxide deposition was confirmed in this study by the observation of metallic Ti when the electrodeposition procedure was performed without an OH^- source. On the other hand, a white TiO_x film was produced when OH^- was locally generated at the ITO electrode by cathodic reduction of H_2O_2 or NO_3^-:[31−33,41]

$$H_2O_2 + 2e^- \rightarrow 2OH^-$$

$$NO_3^- + H_2O + 2e^- \rightarrow NO_2^- + 2OH^-$$

Precipitation of TiO_x from the peroxotitanium precursor was further supported by XPS Ti 2p core level scan (see Figure 3). The spin-orbit split Ti 2p core level photoemission peaks observed at 458.7 and 464.4 eV correspond to Ti^{4+}, and no other oxidation states were observed.[42−44] The lack of change

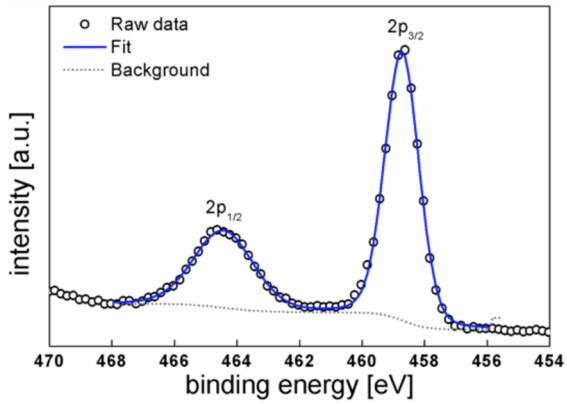

Figure 3. XPS Ti 2p core level spectrum of the as-deposited TiO_x film showing photoemission peaks at 458.7 and 464.4 eV corresponding to Ti^{4+}.

in oxidation state of Ti during the electrodeposition process further confirms precipitation as the dominant deposition mechanism observed.[28]

In aqueous synthesis approaches, TiO_x has been reported to coexist with various forms of hydroxides,[33,37] which are thermally unstable and can be decomposed to form the oxide. To investigate this, XPS analysis was performed on the O 1s photoemission spectra of as-deposited as well as annealed samples (Figure 4). The peaks located at ∼529.8 and ∼531.5

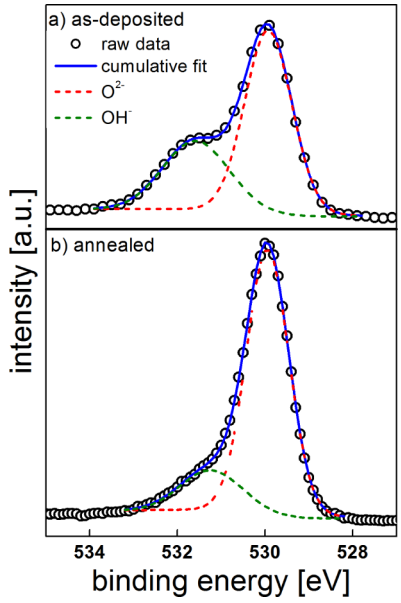

Figure 4. XPS O 1s core level scans of (a) as-deposited and (b) annealed TiO_x samples.

eV correspond to O^{2-} and OH^- bonded to titanium. Quantitative analysis of these peaks revealed a relatively high $Ti(OH)_4$:TiO_x ratio of 1:1.7 and significant O-vacancies (x = 1.56) in the as-deposited films. After annealing in air at 200 °C for 30 min, $Ti(OH)_4$ was observed to decompose partially to TiO_x, increasing the $Ti(OH)_4$:TiO_x ratio to 1:5.9 and O-stoichiometry to x = 1.9. This improved stoichiometry of the TiO_x EEL is desirable for device performance as excess O-vacancies has been shown to suppress charge extraction in OPV.[45] The maximum peak of Ti−OH was slightly, though noticeably, shifted (decreased) after annealing. A similar shift

dx.doi.org/10.1021/am405193r | ACS Appl. Mater. Interfaces 2014, 6, 2679−2685

(increase) was also observed for the Ti−O peak. A slight shift in the binding energy peak of a given chemical species is indicative of a change in its chemical environment. In this case, annealing the sample had caused Ti−OH to dehydrate to form Ti−O. One might imagine that the film starts off as predominantly $Ti(OH)_4$, which then transforms to oxy-hydroxides and oxides upon annealing. We propose the decreasing −OH accompanied by increasing −O was responsible for this change in chemical environment that caused the slight shifts in peak position. Despite these small shifts, we found the peak positions were still within the reported values found in literature.[42]

To quantify the presence of the oxalate impurities, the C contents of the TiO_x films were analyzed and the results are shown in Figure 5. Three distinct deconvoluted emission peaks

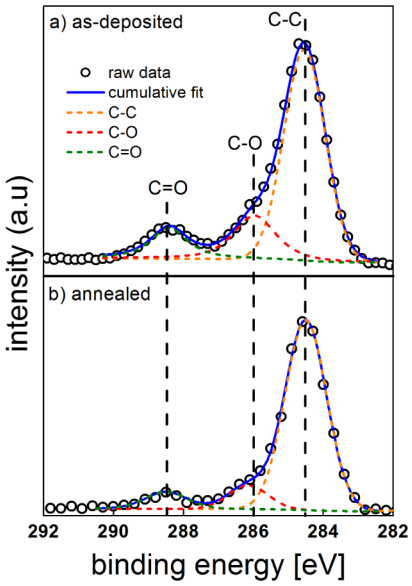

Figure 5. Results of C 1s core level XPS scan of (a) as-deposited and (b) annealed TiO_x samples.

were identified at 284.6, 286, and 288.5 eV corresponding to signatures of the C—C reference peak, C—O, and C═O groups of the oxalate ligand.[46−48] It was firstly noted that oxalate impurity contained in the as-deposited films was moderately low at ∼13%. This strongly suggests that a majority of the oxalate ligands were released back into solution following attack of the electropositive Ti atom by electronegative OH^- ions (Figure 6). Annealing the films further improved the oxalate impurity content to ∼5% by thermal decomposition, thereby increasing purity of the final TiO_x EEL.

Structural Characterization: Morphology. In this study, TiO_x was successfully electroprecipitated using both H_2O_2 and NO_3^- additives. However, the resulting morphology was observed to differ significantly, as revealed by AFM topology measurements of the annealed TiO_x films. In the case of H_2O_2 additives, the film was highly conformal and thus, the substrate was found to have a strong influence on the TiO_x film morphology. Two substrates with different morphologies were used to demonstrate the conformity of the H_2O_2-derived film. Figure 7a,b shows the morphologies of the ITOs used in structural characterization of the electrodeposited TiO_x films (hereafter referred to ITO-a and ITO-b, respectively). The morphology of ITO-a was rice-like whereas ITO-b was defined by plate-like structures and the substrate root-mean-square (RMS) roughness values were 3.5 and 2.5 nm, respectively. Figure 7c,d shows those of H_2O_2-derived TiO_x films deposited on ITO-a and ITO-b, which closely resembled the morphologies of the corresponding substrates. Consequently, the TiO_x films displayed surface roughness that corresponded well with that of the underlying substrate—the RMS roughness of TiO_x films deposited on ITO-a and ITO-b were 3.4 and 1.5 nm, respectively. These images revealed the highly conformal nature of the H_2O_2-derived TiO_x films. On the other hand, when NO_3^- additives were used, the NO_3^--derived TiO_x films (deposited on ITO-b) were extremely rough and did not resemble the substrate morphology. These results suggest that additives have significant influence on the electrodeposited film morphology and the impact of other additives not studied here should be investigated separately. Because smooth interfacial layers are important for achieving intimate electrical contact at the BHJ/TiO_x interface (low series resistance),[18] only H_2O_2 additives were used to deposit TiO_x EEL for device fabrication.

Device Performance. Table 1 tabulates the device performance parameters of ITO/TiO_x/P3HT:PCBM/MoO_x/Al *i*OPVs (Figure 8). The effectiveness of the electrodeposited TiO_x EEL was demonstrated using control devices without any TiO_x EEL. We observed poor photocurrent density (J_{sc}) and open circuit voltage (V_{oc}) in these reference devices. Because V_{oc} is a strong indicator of bulk carrier lifetime, the low V_{oc} observed without the TiO_x EEL, in contrast to over 600 mV at 40 nm TiO_x, clearly indicated the effectiveness of the electroprecipitated TiO_x in passivating carrier recombination (shunt loss) at the ITO electrode. At low TiO_x thicknesses (<10 nm), insufficient coverage of the TiO_x EEL on ITO dominated device performance, giving rise to shunt losses as

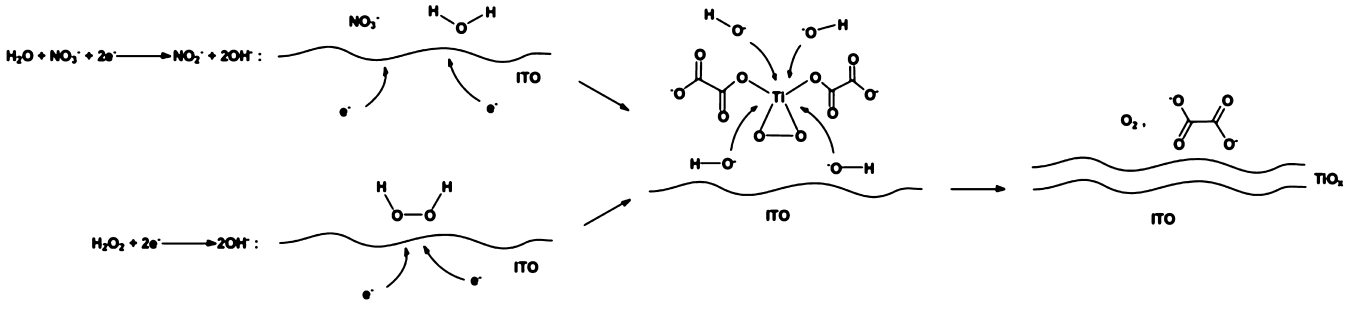

Figure 6. Schematic representation showing the electrogeneration of OH^- from H_2O_2 or NO_3^- additives, molecular structure of the peroxotitanium oxalate precursor and the precipitation mechanism of TiO_x involving the attack of the electropositive Ti atom by OH^- ions, accompanied by release of oxygen and the oxalate ligand back into solution.

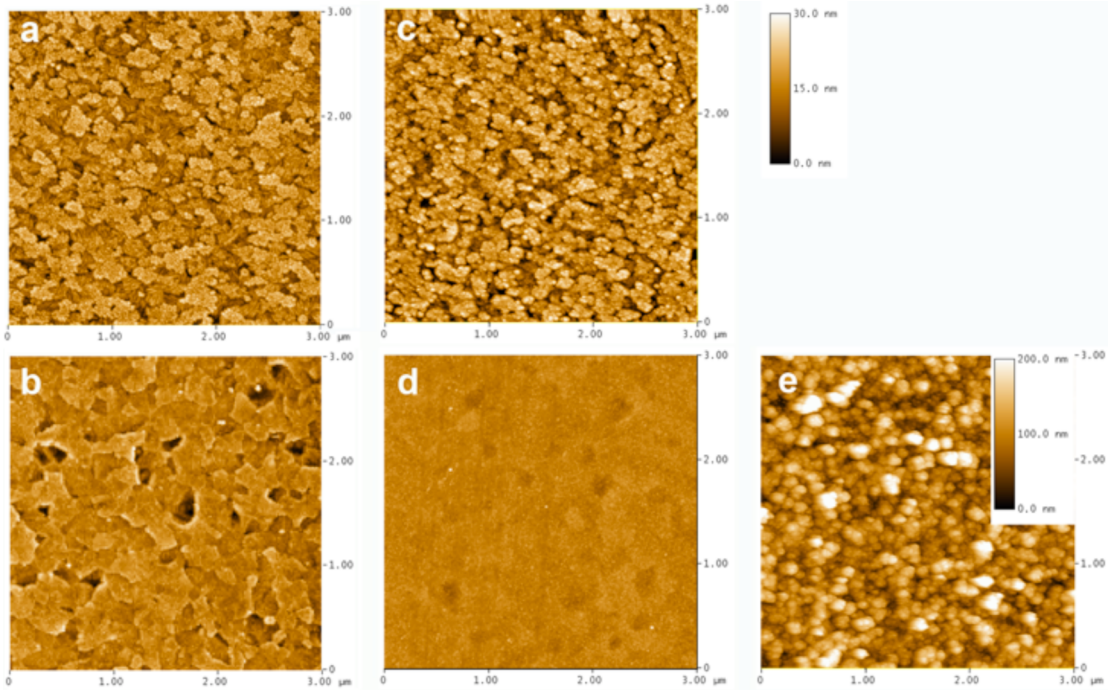

Figure 7. AFM images of (a, b) ITO substrates; (c, d) the corresponding electrodeposited TiO_x films (50 nm) with H_2O_2 additive and (e) TiO_x films with NO_3^- additive (the height bar for a-d is given in the top right whereas that for image e is given in inset).

Table 1. Device Performance Parameters of ITO/TiO_x/P3HT:PCBM/MoO_x (5 nm)/Al *i*OPV Devices Presented against TiO_x Thickness[a]

TiO_x thickness (nm)	V_{oc} (±20 mV)	J_{sc} (±0.4 mA cm^{-2})	FF (±5%)	η (±0.3%)	R_{sh} (kΩ cm^2)	R_s (Ω cm^2)
0	330	2.1	31.5	0.22		
5	350	6.8	32.7	0.78	0.4	14.2
10	535	8.7	36.2	1.7	0.6	21.8
20	578	10.4	47.3	2.8	0.9	10.5
40	610	10.6	59	3.8	1.4	8.4
100	591	10.5	53.2	3.3	1.9	15.7
120	580	10.4	50.4	3.0	2.2	17.9

[a]Shunt (R_{sh}) and series (R_s) resistance values were extracted graphically.

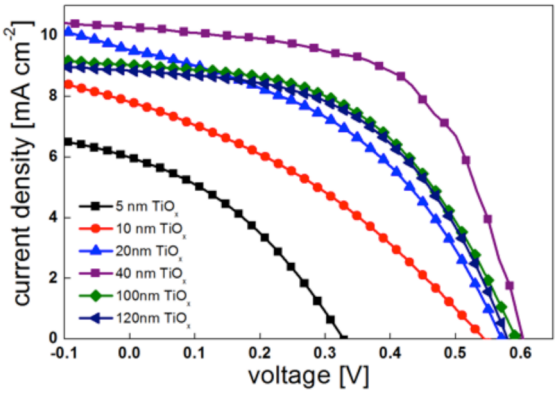

Figure 8. Measured J−V curve of ITO/TiO_x/P3HT:PCBM/5 nm MoO_x/Al *i*OPV devices.

revealed by low R_{sh} values (<1 kΩ cm^2). By gradually increasing the TiO_x EEL thickness, TiO_x coverage over the ITO substrate improved, giving rise to high R_{sh} values that stabilized at around 1.4−2.2 kΩ cm^2. Correspondingly, R_s decreased from 21.8 to 8.4 Ω cm^2. When the TiO_x thickness approached 40 nm, we observed dramatic improvements in V_{oc}, J_{sc}, and FF up to a maximum of efficiency of 3.8%, V_{oc} of 610 mV, J_{sc} of 10.6 mA cm^{-2}, and FF of 59%. Further increases in TiO_x mainly affected FF due to increasing R_s. The high J_{sc} observed could be attributed to the high transmittance of the TiO_x films recorded (Supporting Information, Figure S2 and Table S1). These results gave good indication of the capacity of the electro-precipitated TiO_x EEL in effectively enhancing all important *i*OPV device parameters by minimizing shunt losses to yield efficient *i*OPV devices.

The MoO_x HEL used in the aforementioned devices were thermally evaporated. Because it is attractive to solution process the HEL as well, *i*OPV devices incorporating the electro-deposited TiO_x EEL were fabricated with spin coated PEDOT:PSS HEL. The PEDOT:PSS HEL was modified with 5% vol FS-31 fluorosurfactant (PEDOT:PSS-FS31) to ensure good wettability of the water-based PEDOT:PSS on the hydrophobic BHJ layer. The device performances of the ITO/40 nm TiO_x/P3HT:PCBM/40 nm PEDOT:PSS-FS31/Ag device are presented in Table 2. Considering overall device performance, the ITO/TiO_x/P3HT:PCBM/PEDOT:PSS-FS31/Ag devices achieved comparable J_{sc} and FF but lower V_{oc} than ITO/TiO_x/P3HT:PCBM/MoO_x/Al devices. Interestingly, we observed significantly higher J_{sc} and lower V_{oc} values

Table 2. Device Performance Parameters of ITO/TiO_x (40 nm)/P3HT:PCBM/PEDOT:PSS-FS31 (40 nm)/Ag Device Incorporating Fully Solution Processed TiO_x and PEDOT:PSS Interfacial Layers

device	V_{oc} (mV)	J_{sc} (mA cm^{-2})	FF (%)	η (%)
ITO/TiO_x/P3HT:PCBM/PEDOT:PSS/Ag	558	10.1	60.4	3.40

using the electrodeposited TiO_x than those reported by Lim et al., who first reported the use of PEDOT:SS-FS31 with sol-gel TiO_x.[39] It is hypothesized that careful removal of the FS-31 surfactant is necessary to achieve high V_{oc} while further studies to understand the advantage of using electrodeposited TiO_x on J_{sc} are ongoing. Nevertheless, the results achieved here demonstrated the versatility of the electrodeposited TiO_x EEL for various HEL.

CONCLUSIONS

In summary, a low temperature electrodeposition process using an aqueous, air stable peroxotitanium precursor was used to prepare TiO_x EEL for *i*OPVs. Thin TiO_x films ranging from 5 to 180 nm were found to deposit readily on ITO substrates upon electrogeneration of OH^- ions through appropriate additives (H_2O_2 and NO_3^-) that greatly influenced the morphology of the TiO_x films. It was found that H_2O_2 additives produced highly conformal TiO_x films which, when coated on low roughness substrates, produced extremely smooth TiO_x films. Conversely, significantly rougher films with spherical growths were obtained using a NO_3^- additive, which suggests that the choice of additive has a significant impact on film morphology. Elemental analysis of the as-deposited films suggested that ligand substitution with OH^- groups to result in TiO_x precipitation was the dominant mechanism for film deposition. A low temperature heat treatment in air was found to reduce oxalate ligand and hydroxide impurities and improve the O stoichiometry of the TiO_x films. Efficient ITO/TiO_x/P3HT:PCBM/MoO_x/Al devices incorporating the TiO_x EEL and thermally evaporated MoO_x HEL were used to demonstrate the effectiveness of the electrodeposited TiO_x films in enhancing *i*OPV performance. The compatibility of the electrodeposited TiO_x EEL with solution processed HEL was investigated as well using a surfactant modified PEDOT:PSS HEL.

ASSOCIATED CONTENT

Supporting Information

Additional figures of electrode setup, optical transmittance spectra and weight average transmittance of films. This material is available free of charge via the Internet at http://pubs.acs.org.

AUTHOR INFORMATION

Corresponding Authors

*K. H. Wong. E-mail:kimhai.wong@nus.edu.sg.
*J. Ouyang. E-mail: mseoj@nus.edu.sg.
*P. Balaya. E-mail: mpepb@nus.edu.sg.

Present Addresses

[⊥]TUM CREATE, 1 CREATE Way, Singapore 138602, Singapore
[∥]School of Chemical and Biotechnology, SASTRA University, Thanjavur 613401, India

Notes

The authors declare no competing financial interest.

ACKNOWLEDGMENTS

The authors gratefully acknowledge the Singapore National Research Foundation (Energy Innovation Programme Office) for Ph.D. scholarship awarded to K. H. Wong and Chin Yong Neo for enlightening scientific discussions. The Solar Energy Research Institute of Singapore is sponsored by the National University of Singapore and the National Research Foundation, through the Singapore Economic Development Board.

REFERENCES

(1) Clarke, T. M.; Durrant, J. R. Charge Photogeneration in Organic Solar Cells. *Chem. Rev.* **2010**, *110*, 6736−6767.
(2) Pagliaro, M.; Ciriminna, R.; Palmisano, G. Flexible Solar Cells. *ChemSusChem* **2008**, *1*, 880−891.
(3) Kaltenbrunner, M.; White, M. S.; Głowacki, E. D.; Sekitani, T.; Someya, T.; Sariciftci, N. S.; Bauer, S. Ultrathin and Lightweight Organic Solar Cells with High Flexibility. *Nat. Commun.* **2012**, *3*, 770.
(4) Angmo, D.; Larsen-Olsen, T. T.; Jørgensen, M.; Søndergaard, R. R.; Krebs, F. C. Roll-to-Roll Inkjet Printing and Photonic Sintering of Electrodes for ITO Free Polymer Solar Cell Modules and Facile Product Integration. *Adv. Energy Mater* **2012**, 172−175.
(5) Espinosa, N.; Garcia-Valverde, R.; Krebs, F. C. Life-Cycle Analysis of Product Integrated Polymer Solar Cells. *Energy Environ. Sci.* **2011**, *4*, 1547−1557.
(6) Ratcliff, E. L.; Zacher, B.; Armstrong, N. R. Selective Interlayers and Contacts in Organic Photovoltaic Cells. *J. Phys. Chem. Lett.* **2011**, *2*, 1337−1350.
(7) Chen, L.-M.; Xu, Z.; Hong, Z.; Yang, Y. Interface Investigation and Engineering - Achieving High Performance Polymer Photovoltaic Devices. *J. Mater. Chem.* **2010**, *20*, 2575−2598.
(8) Steim, R.; Kogler, F. R.; Brabec, C. J. Interface Materials for Organic Solar Cells. *J. Mater. Chem.* **2010**, *20*, 2499−2512.
(9) de Jong, M. P.; van Ijzendoorn, L. J.; de Voigt, M. J. A. Stability of the Interface between Indium-Tin-Oxide and Poly(3,4-ethylenedioxythiophene)/Poly(styrenesulfonate) in Polymer Light-Emitting Diodes. *Appl. Phys. Lett.* **2000**, *77*, 2255−2257.
(10) Kuwabara, T.; Nakayama, T.; Uozumi, K.; Yamaguchi, T.; Takahashi, K. Highly Durable Inverted-Type Organic Solar Cell Using Amorphous Titanium Oxide as Electron Collection Electrode Inserted between ITO and Organic Layer. *Sol. Energy Mater. Sol. Cells* **2008**, *92*, 1476−1482.
(11) Jørgensen, M.; Norrman, K.; Krebs, F. C. Stability/Degradation of Polymer Solar Cells. *Sol. Energy Mater. Sol. Cells* **2008**, *92*, 686−714.
(12) Wong, K. H.; Ananthanarayanan, K.; Heinemann, M. D.; Luther, J.; Balaya, P. Enhanced Photocurrent and Stability of Organic Solar Cells using Solution-based NiO Interfacial Layer. *Sol. Energy* **2012**, *86*, 3190−3195.
(13) Wong, K. H.; Ananthanarayanan, K.; Luther, J.; Balaya, P. Origin of Hole Selectivity and the Role of Defects in Low-Temperature Solution-Processed Molybdenum Oxide Interfacial Layer for Organic Solar Cells. *J. Phys. Chem. C* **2012**, *116*, 16346−16351.
(14) Jeong, S.; Moon, J. Low-temperature, Solution-processed Metal Oxide Thin Film Transistors. *J. Mater. Chem.* **2012**, *22*, 1243−1250.
(15) Mohd Yusoff, A. R. b.; Kim, H. P.; Jang, J. Inverted Organic Solar Cells with TiO_x Cathode and Graphene Oxide Anode Buffer Layers. *Sol. Energy Mater. Sol. Cells* **2013**, *109*, 63−69.
(16) Wang, M.; Li, Y.; Huang, H.; Peterson, E. D.; Nie, W.; Zhou, W.; Zeng, W.; Huang, W.; Fang, G.; Sun, N.; Zhao, X.; Carroll, D. L. Thickness Dependence of the MoO_3 Blocking Layers on ZnO Nanorod-Inverted Organic Photovoltaic Devices. *Appl. Phys. Lett.* **2011**, *98*, 103305.
(17) Lin, Z.; Jiang, C.; Zhu, C.; Zhang, J. Development of Inverted Organic Solar Cells with TiO_2 Interface Layer by Using Low-Temperature Atomic Layer Deposition. *ACS Appl. Mater. Interfaces* **2013**, *5*, 713−718.

(18) Liang, Z.; Zhang, Q.; Wiranwetchayan, O.; Xi, J.; Yang, Z.; Park, K.; Li, C.; Cao, G. Effects of the Morphology of a ZnO Buffer Layer on the Photovoltaic Performance of Inverted Polymer Solar Cells. *Adv. Funct. Mater.* **2012**, *22*, 2194−2201.
(19) Trost, S.; Zilberberg, K.; Behrendt, A.; Riedl, T. Room-temperature Solution Processed SnO_x as an Electron Extraction Layer for Inverted Organic Solar Cells with Superior Thermal Stability. *J. Mater. Chem.* **2012**, *22*, 16224−16229.
(20) Seo, H. O.; Park, S.-Y.; Shim, W. H.; Kim, K.-D.; Lee, K. H.; Jo, M. Y.; Kim, J. H.; Lee, E.; Kim, D.-W.; Kim, Y. D.; Lim, D. C. Ultrathin TiO_2 Films on ZnO Electron-Collecting Layers of Inverted Organic Solar Cell. *J. Phys. Chem. C* **2011**, *115*, 21517−21520.
(21) Sun, H.; Weickert, J.; Hesse, H. C.; Schmidt-Mende, L. UV Light Protection Through TiO_2 Blocking Layers for Inverted Organic Solar Cells. *Sol. Energy Mater. Sol. Cells* **2011**, *95*, 3450−3454.
(22) Sun, Y.; Seo, J. H.; Takacs, C. J.; Seifter, J.; Heeger, A. J. Inverted Polymer Solar Cells Integrated with a Low-Temperature-Annealed Sol-Gel-Derived ZnO Film as an Electron Transport Layer. *Adv. Mater.* **2011**, *23*, 1679−1683.
(23) Wang, J.-C.; Weng, W.-T.; Tsai, M.-Y.; Lee, M.-K.; Horng, S.-F.; Perng, T.-P.; Kei, C.-C.; Yu, C.-C.; Meng, H.-F. Highly Efficient Flexible Inverted Organic Solar Cells Using Atomic Layer Deposited ZnO as Electron Selective Layer. *J. Mater. Chem.* **2010**, *20*, 862−866.
(24) Voigt, M. M.; Mackenzie, R. C. I.; Yau, C. P.; Atienzar, P.; Dane, J.; Keivanidis, P. E.; Bradley, D. D. C.; Nelson, J. Gravure Printing for Three Subsequent Solar Cell Layers of Inverted Structures on Flexible Substrates. *Sol. Energy Mater. Sol. Cells* **2011**, *95*, 731−734.
(25) Hadipour, A.; Müller, R.; Heremans, P. Room Temperature Solution-Processed Electron Transport Layer for Organic Solar Cells. *Org. Electron.* **2013**, *14*, 2379−2386.
(26) Savva, A.; Petraki, F.; Elefteriou, P.; Sygellou, L.; Voigt, M.; Giannouli, M.; Kennou, S.; Nelson, J.; Bradley, D. D. C.; Brabec, C. J.; Choulis, S. A. The Effect of Organic and Metal Oxide Interfacial Layers on the Performance of Inverted Organic Photovoltaics. *Adv. Energy Mater* **2013**, *3*, 391−398.
(27) Bennett, J. A.; Iii, J. E. P.; Neiswonger, M. A. Investigating the Viability of Electrodeposited Vanadium Pentoxide as a Suitable Electrode Material for in-Vivo Amperometric Hydrogen Sulfide Detection. *J. Electroanal. Chem.* **2011**, *654*, 1−7.
(28) Pauporté, T.; Goux, A.; Kahn-Harari, A.; De Tacconi, N.; Chenthamarakshan, C. R.; Rajeshwar, K.; Lincot, D. Cathodic Electrodeposition of Mixed Oxide Thin Films. *J. Phys. Chem. Solids* **2003**, *64*, 1737−1742.
(29) Koura, N.; Tsukamoto, T.; Shoji, H.; Hotta, T. Preparation of Various Oxide Films by an Electrophoretic Deposition Method: A Study of the Mechanism. *Jpn. J. Appl. Phys.* **1995**, *34*, 1643.
(30) Sarkar, P.; Nicholson, P. S. Electrophoretic Deposition (EPD): Mechanisms, Kinetics, and Application to Ceramics. *J. Am. Ceram. Soc.* **1996**, *79*, 1987−2002.
(31) Yoshida, T.; Tochimoto, M.; Schlettwein, D.; Wöhrle, D.; Sugiura, T.; Minoura, H. Self-Assembly of Zinc Oxide Thin Films Modified with Tetrasulfonated Metallophthalocyanines by One-Step Electrodeposition. *Chem. Mater.* **1999**, *11*, 2657−2667.
(32) Matsumoto, Y.; Ishikawa, Y.; Nishida, M.; Ii, S. A New Electrochemical Method To Prepare Mesoporous Titanium(IV) Oxide Photocatalyst Fixed on Alumite Substrate. *J. Phys. Chem. B* **2000**, *104*, 4204−4209.
(33) Natarajan, C.; Nogami, G. Cathodic Electrodeposition of Nanocrystalline Titanium Dioxide Thin Films. *J. Electrochem. Soc.* **1996**, *143*, 1547−1550.
(34) Miyasaka, T.; Kijitori, Y. Low-Temperature Fabrication of Dye-Sensitized Plastic Electrodes by Electrophoretic Preparation of Mesoporous TiO_2 Layers. *J. Electrochem. Soc.* **2004**, *151*, A1767−A1773.
(35) Benehkohal, N. P.; Demopoulos, G. P. Green Preparation of TiO_2-ZnO Nanocomposite Photoanodes by Aqueous Electrophoretic Deposition. *J. Electrochem. Soc.* **2012**, *159*, B602−B610.
(36) Kuwabara, T.; Sugiyama, H.; Yamaguchi, T.; Takahashi, K. Inverted Type Bulk-heterojunction Organic Solar Cell Using Electrodeposited Titanium Oxide Thin Films as Electron Collector Electrode. *Thin Solid Films* **2009**, *517*, 3766−3769.
(37) Karuppuchamy, S.; Nonomura, K.; Yoshida, T.; Sugiura, T.; Minoura, H. Cathodic Electrodeposition of Oxide Semiconductor Thin Films and Their Application to Dye-Sensitized Solar Cells. *Solid State Ionics* **2002**, *151*, 19−27.
(38) Connor, J. A.; Ebsworth, E. A. V. Peroxy Compounds of Transition Metals. In *Advances in Inorganic Chemistry and Radiochemistry*; Emeléus, H. J., Sharpe, A. G., Eds.; Academic Press: New York, 1964; Vol. *6*, pp 279−381.
(39) Lim, F. J.; Ananthanarayanan, K.; Luther, J.; Ho, G. W. Influence of a Novel Fluorosurfactant Modified PEDOT:PSS Hole Transport Layer on the Performance of Inverted Organic Solar Cells. *J. Mater. Chem.* **2012**, *22*, 25057−25064.
(40) Muehlebach, J.; Mueller, K.; Schwarzenbach, G. Peroxo Complexes of Titanium. *Inorg. Chem.* **1970**, *9*, 2381−2390.
(41) Zhitomirsky, I.; Gal-Or, L. Cathodic Electrosynthesis of Ceramic Deposits. *J. Eur. Ceram. Soc.* **1996**, *16*, 819−824.
(42) Sanjines, R.; Tang, H.; Berger, H.; Gozzo, F.; Margaritondo, G.; Levy, F. Electronic Structure of Anatase TiO_2. *J. Appl. Phys.* **1994**, *75*, 2945−2951.
(43) Sedona, F.; Rizzi, G. A.; Agnoli, S.; Llabres i Xamena, F. X.; Papageorgiou, A.; Ostermann, D.; Sambi, M.; Finetti, P.; Schierbaum, K.; Granozzi, G. Ultrathin TiO_x Films on Pt(111): A LEED, XPS, and STM Investigation. *J. Phys. Chem. B* **2005**, *109*, 24411−24426.
(44) Södergren, S.; Siegbahn, H.; Rensmo, H.; Lindström, H.; Hagfeldt, A.; Lindquist, S.-E. Lithium Intercalation in Nanoporous Anatase TiO2 Studied with XPS. *J. Phys. Chem. B* **1997**, *101*, 3087−3090.
(45) Kim, J.; Kim, G.; Choi, Y.; Lee, J.; Park, S. H.; Lee, K. Light-soaking Issue in Polymer Solar Cells: Photoinduced Energy Level Alignment at the Sol-Gel Processed Metal Oxide and Indium Tin Oxide Interface. *J. Appl. Phys.* **2012**, *111*, 114511.
(46) Papirer, E.; Lacroix, R.; Donnet, J.-B.; Nanse, G.; Fioux, P. XPS Study of the Halogenation of Carbon Black, Part 1. Bromination. *Carbon* **1994**, *32*, 1341−1358.
(47) Papirer, E.; Lacroix, R.; Donnet, J.-B.; Nanse, G.; Fioux, P. XPS Study of the Halogenation of Carbon Black, Part 2. Chlorination. *Carbon* **1995**, *33*, 63−72.
(48) Clark, D. T.; Thomas, H. R. Applications of ESCA to Polymer Chemistry. XI. Core and Valence Energy Levels of a Series of Polymethacrylates. *J. Polym. Sci., Polym. Chem. Ed.* **1976**, *14*, 1701−1713.